Supporting Information

What happens in the dark? Assessing the temporal control of photo-mediated controlled radical polymerizations

Neil D. Dolinski, Zachariah A. Page, Emre H. Discekici, David Meis, In-Hwan Lee, Glen R. Jones, Richard Whitfield, Xiangcheng Pan, Blaine G. McCarthy, Sivaprakash Shanmugam, Veronika Kottisch, Brett P. Fors, Cyrille Boyer, Garret M. Miyake, Krzysztof Matyjaszewski, David M. Haddleton, Javier Read de Alaniz, Athina Anastasaki*, Craig J. Hawker*

Corresponding author: *hawker@mrl.ucsb.edu, *athina@cnsi.ucsb.edu

Table of Contents

Experimental Details

Materials

All materials were purchased from Sigma Aldrich and used as received unless otherwise stated. All deuterated solvents were purchased from Fisher Scientific and used as received. Methyl acrylate (MA), methyl methacrylate (MMA), and polyethyleneglycol acrylate (M_n ~400) were passed through a column of basic alumina (~150 mesh, Brockmann I grade) prior to use in order to remove the inhibitor. 3,7-di(4-biphenyl) 1-naphthalene-10-phenoxazine (PhenBP)[1], 10-phenylphenothiazine (PTH)[2], and [Cu(Me6-Tren)(O2CH)](ClO4)[3] were synthesized according to literature procedures. The Teflon insert was machined in house according to literature.[4] The optical fiber (FT1000UMT; End A flat cleave; End BSMA adapter; Furcation Tubing-FT038), and the fiber-coupled LEDs 365 nm (M365FP1), 405 nm (M405FP1), 470 nm (M470F3), 530 nm (M530F2), were purchased from Thorlabs.

Instrumentation

All nuclear magnetic resonance spectra were recorded on a Varian 600 MHz spectrometer with a regulated temperature of 25 °C. Size exclusion chromatography (SEC) for molecular weight analysis, relative to linear polystyrene standards, was performed on a Waters 2690 separation module equipped with Waters 2414 refractive index and 2996 photodiode array detectors using $CHCl_3$-containing 0.25% triethylamine as eluent at a flow rate of 1 mL/min. For photopolymerizations in the NMR spectrometer, the LED was coupled into a multimode optical fiber terminated with a flat cleave and the intensity and 'on' / 'off' cycles were controlled through methods described previously.[4]

Sample preparation

Polymerizations were prepared in 1 dram vials with 33% monomer targeting 150 repeat units (~1.5 mL batches). Catalytic loadings were chosen as appropriate from the corresponding literature. After mixing, the samples were sparged with Ar for 5 minutes prior to transfer into a foiled NMR tube (Ar atmosphere provided via balloon). The foil was removed and the NMR tube was then quickly loaded with the optical fiber and inserted into the NMR for measurement.

LED selection

Excitation wavelengths were chosen such that the calculated absorbance for a sample at 1 cm (using Beer's Law) was maximized, but below 0.25, as recommended in previous work[4] to ensure even irradiation conditions. In the case of highly absorbing catalysts, or the presence of a large UV shoulder, LEDs with output maxima slightly shifted from the peak/shoulder were chosen to satisfy the absorbance requirements.

Table S1: LEDs used for each catalyst studied

Catalyst System	Solvent	LED (nm)
$Ru(bpy)_3Cl_2$	DMSO-d_6	470
ZnTPP	DMSO-d_6	530
PTH	DMF-d_7	405
$Ir(ppy)_3$	DMF-d_7	405
PhenBP	DMF-d_7	470
$CuBr_2$/Me_6TREN	DMSO-d_6/DMF-d_7	405
$CuBr_2$/Me_6TREN	D_2O	365
Cu-Formate Complex	DMSO-d_6	365
$CuBr_2$/TPMA	DMSO-d_6	405

Fiber-coupled NMR setup

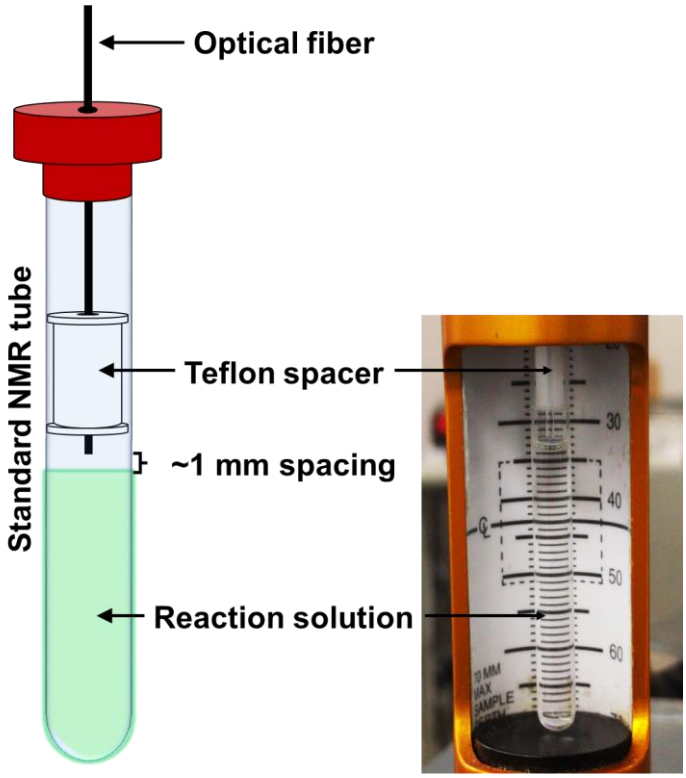

Figure S1: (Left) Cartoon schematic of the fiber-coupled NMR setup. (Right) Photograph of the 'active' portion of the setup, where the Teflon spacer centers the tip of the optical fiber ~1 mm from the top of the reaction solution. Full details on spacer dimensions and necessary hardware for operation given in previous work.[4]

NMR processing

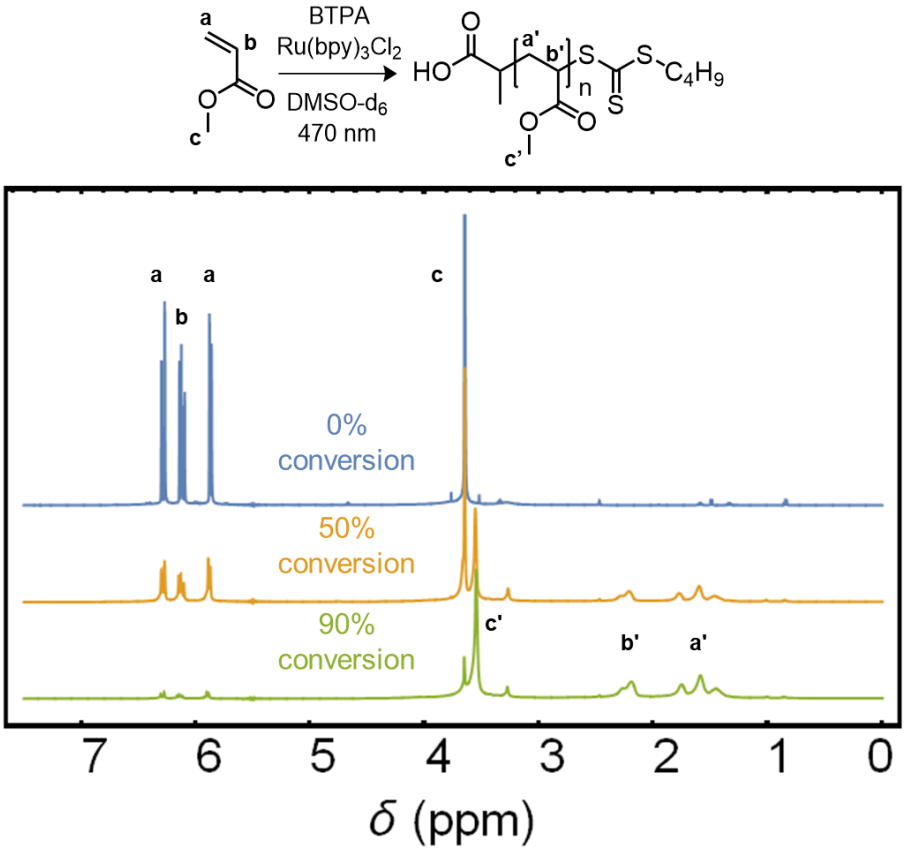

Figure S2: Representative ^{1}H-NMR spectra for the polymerization of MA by PET-RAFT at various stages of conversion. Peaks labeled a, a', b, and b' were used for calculations according to the formula shown below. Additional peaks are labeled for completion.

$$Conversion = \frac{\int Peaks\ a', b'}{\int Peaks\ a, b + \int Peaks\ a', b'}$$

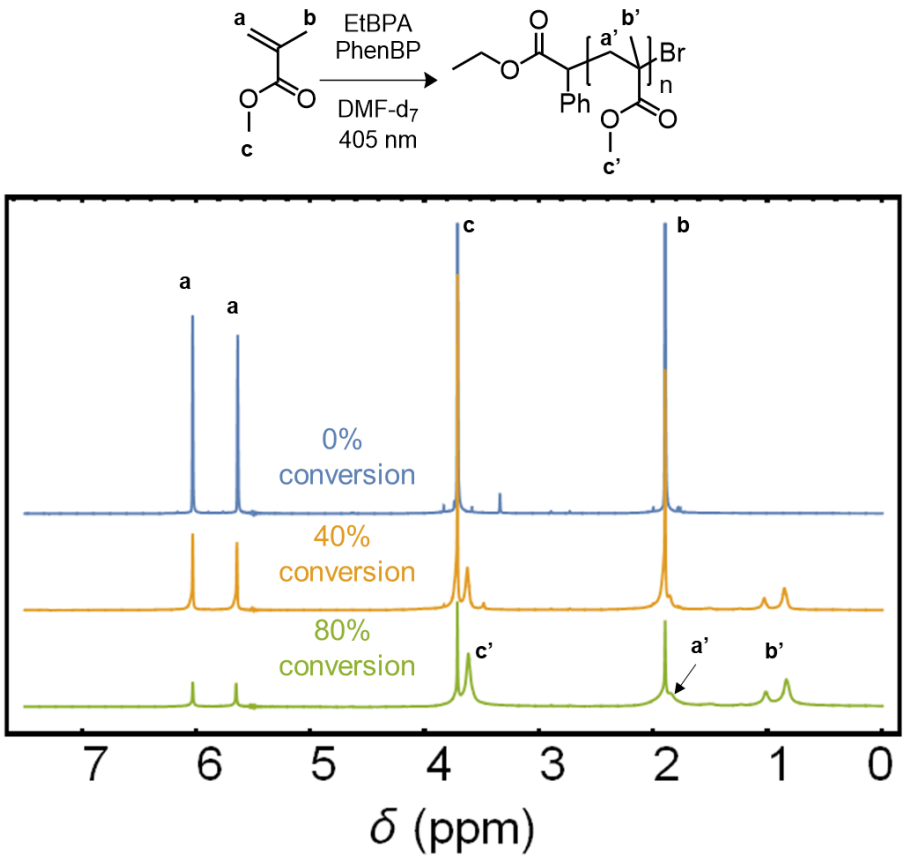

Figure S3: Representative ^{1}H-NMR spectra for the polymerization of MMA by Cu-free ATRP at various stages of conversion. Peaks labeled a and b' were used for calculations according to the formula shown below. Additional peaks are labeled for completion.

$$Conversion = \frac{\frac{2}{3}\int Peaks\ b'}{\int Peaks\ a + \frac{2}{3}\int Peaks\ b'}$$

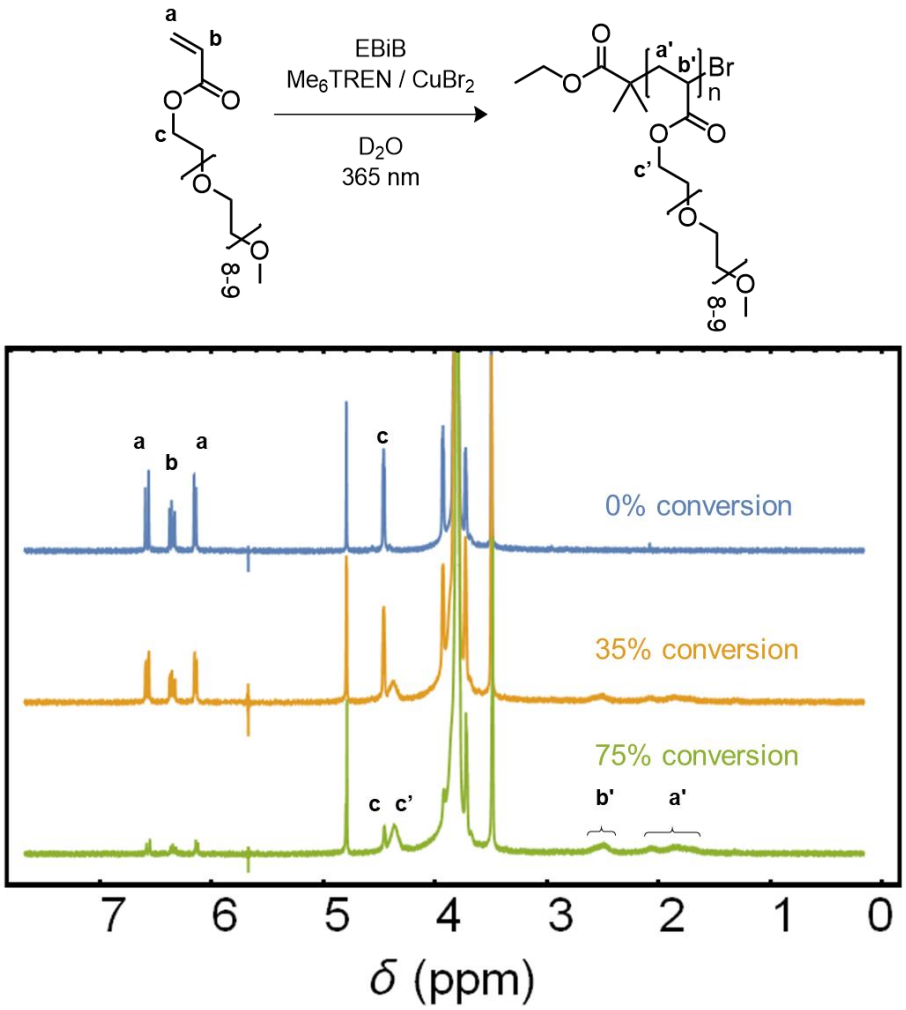

Figure S4: Representative ^{1}H-NMR spectra for the polymerization of PEGA by Cu-mediated RDRP (aqueous) at various stages of conversion. Peaks labeled a, b, c, and c' were used for calculations according to the formula shown below. Additional peaks are labeled for completion.

$$Conversion = 1 - \frac{\frac{2}{3}\int Peaks\ a, b}{\int Peaks\ c, c'}$$

Characterization

LED outputs

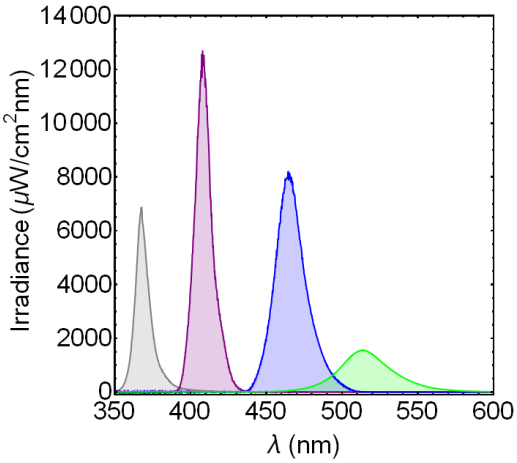

Figure S5: Irradiance measurements of the various LEDs (365, 405, 470, and 530 nm) used in this work at 100% current.

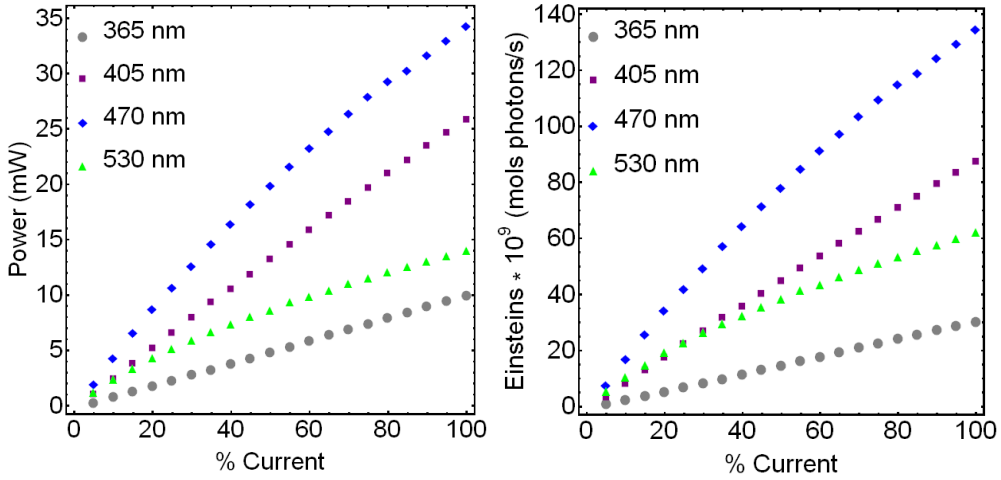

Figure S6: (Left) Power measurements for the fiber coupled LEDs at various supplied currents. (Right) The power measurements converted to photon flux (see equation below). All experiments were run such that the photon flux was constant (using the value for the weakest LED at 100% current).

$$Photon\ flux\ (Einsteins) = \frac{P * \lambda}{h * c * N_A}$$

Where P is LED power (W), λ is peak LED wavelength (m), h is Planck's constant (J·s), c is the speed of light (m/s), and N_A is Avogadro's Number

Table S2: Irradiation conditions used in this study with constant photon flux

LED wavelength (nm)	Current for equal photon flux (%)
365	100
405	34.0
470	17.7
530	36.6

Catalyst absorption profiles

PET-RAFT

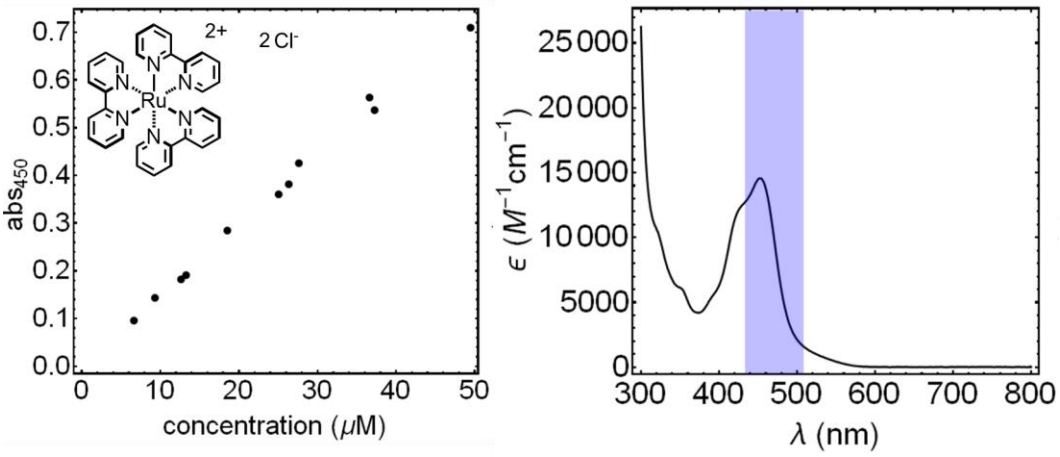

Figure S7: (Left) UV-vis measurements to determine the molar extinction coefficient of $Ru(bpy)_3Cl_2$ in DMSO. (Right) Trace of the calculated extinction for $Ru(bpy)_3Cl_2$ and overlap with 470 nm light.

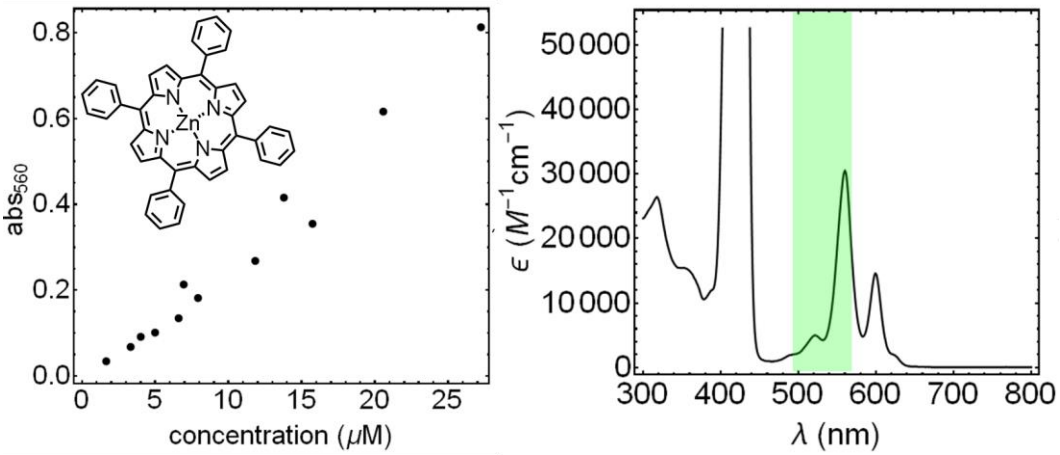

Figure S8: (Left) UV-vis measurements to determine the molar extinction coefficient of ZnTPP in DMSO. (Right) Trace of the calculated extinction for ZnTPP and overlap with 530 nm light.

Cu-free ATRP

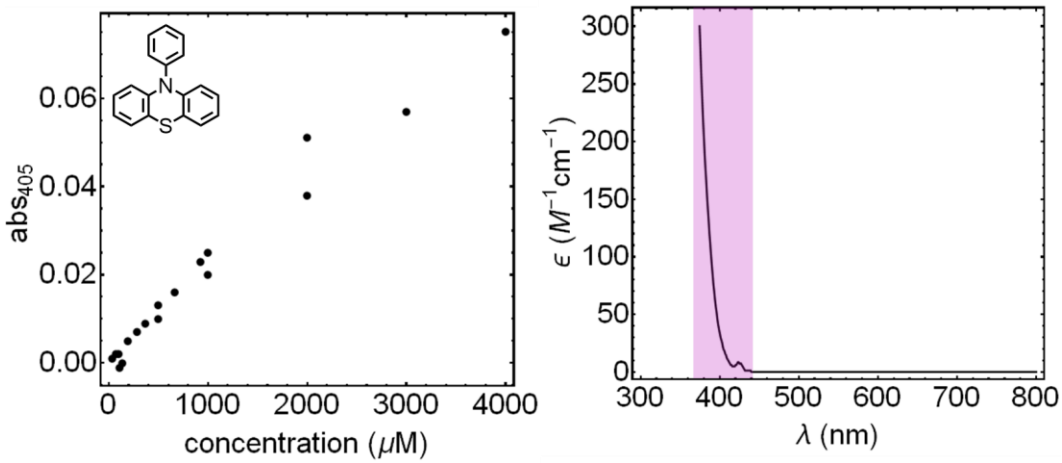

Figure S9: (Left) UV-vis measurements to determine the molar extinction coefficient of PTH in DMF. (Right) Trace of the calculated extinction for PTH and overlap with 405 nm light.

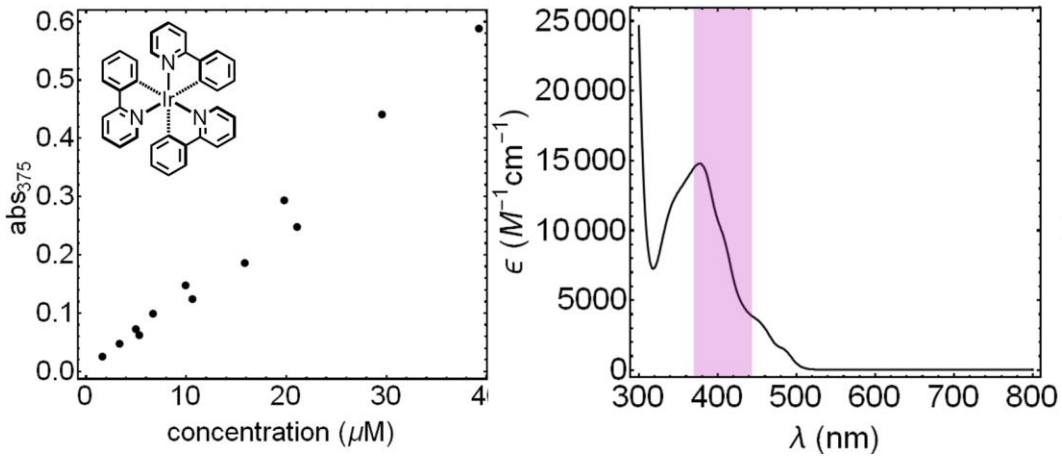

Figure S10: (Left) UV-vis measurements to determine the molar extinction coefficient of $Ir(ppy)_3$ in DMF. (Right) Trace of the calculated extinction for $Ru(bpy)_3Cl_2$ and overlap with 405 nm light.

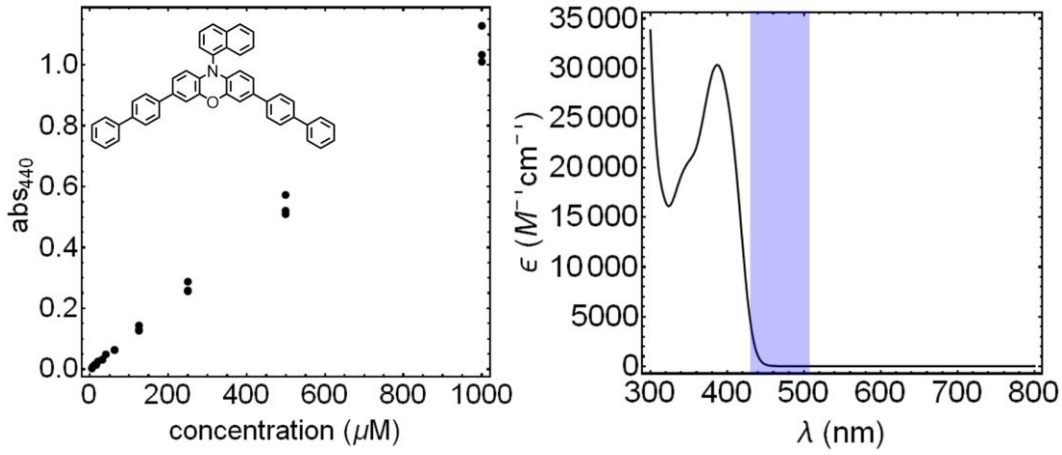

Figure S11: (Left) UV-vis measurements to determine the molar extinction coefficient of PhenBP in DMF. (Right) Trace of the calculated extinction for PhenBP and overlap with 470 nm light.

Cu-mediated RDRP

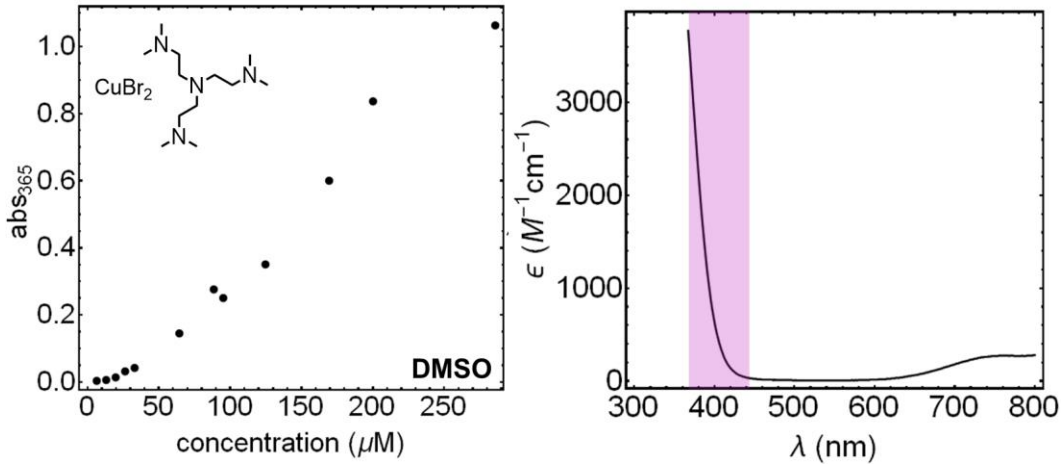

Figure S12: (Left) UV-vis measurements to determine the molar extinction coefficient of $CuBr_2$ / Me_6TREN in DMSO. (Right) Trace of the calculated extinction for $CuBr_2$ / Me_6TREN and overlap with 405 nm light.

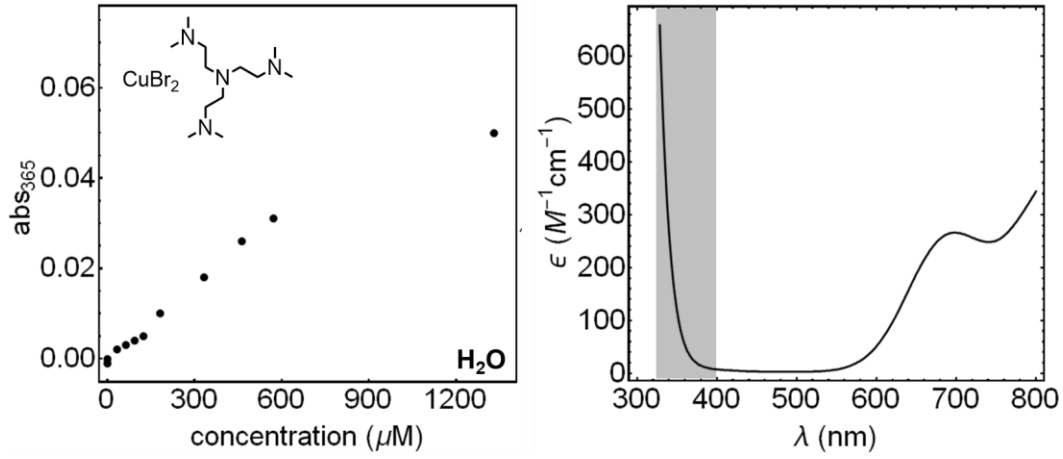

Figure S13: (Left) UV-vis measurements to determine the molar extinction coefficient of $CuBr_2$ / Me_6TREN in H_2O. (Right) Trace of the calculated extinction for $CuBr_2$ / Me_6TREN and overlap with 365 nm light. It should be noted that moving to water significantly shifted the absorbances relative to DMSO, necessitating the use of 365 nm light.

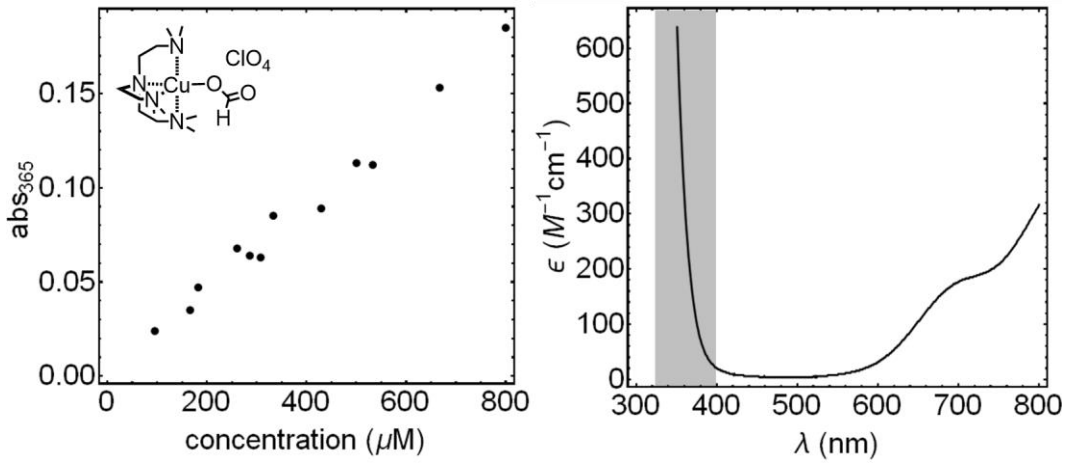

Figure S14: (Left) UV-vis measurements to determine the molar extinction coefficient of [Cu(Me6-Tren)(O2CH)](ClO4), the Cu-formate complex, in DMSO. (Right) Trace of the calculated extinction for the Cu-formate complex and overlap with 365 nm light.

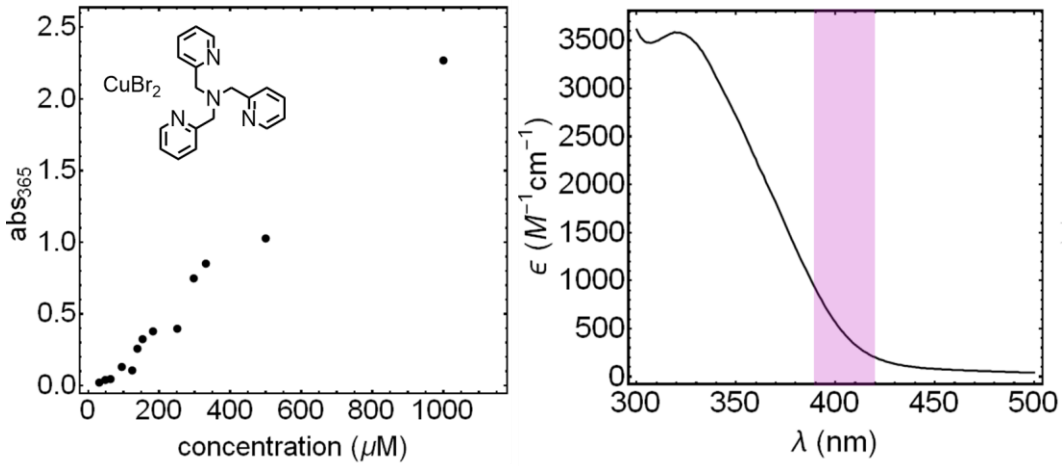

Figure S15: (Left) UV-vis measurements to determine the molar extinction coefficient of $CuBr_2$ / TPMA in DMSO. (Right) Trace of the calculated extinction for $CuBr_2$ / TPMA and overlap with 405 nm light.

Polymerization kinetics, cycling experiments, and extended 'off' periods

PET-RAFT (MA)

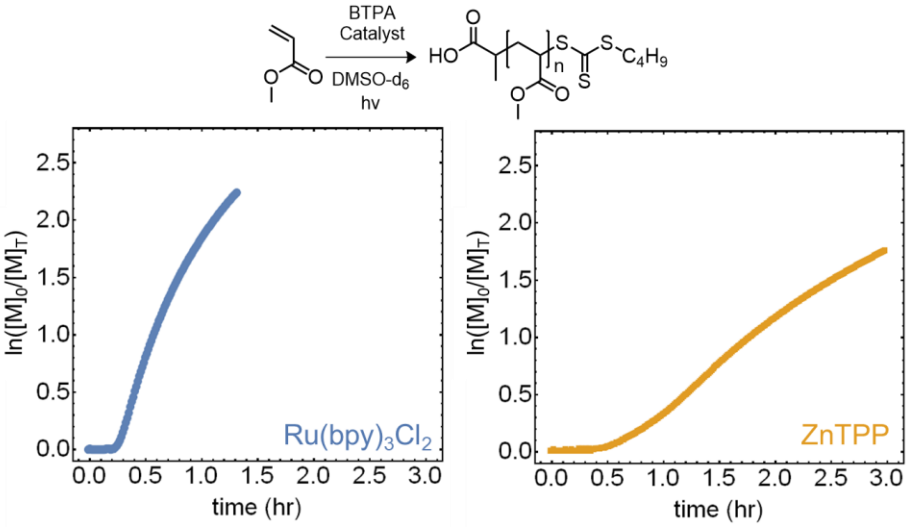

Figure S16: Kinetic traces of PET-RAFT polymerizations of MA using $Ru(bpy)_3Cl_2$ (left) and ZnTPP (right) under 470 and 530 nm irradiation, respectively.

Table S3: Summary of PET-RAFT polymerizations of MA and results

catalyst	λ (nm)	[M]:[I]:[catalyst]	time (hr)	conversion	$M_{n,theo}$	$M_{n,exp}$ (SEC)	Đ
$Ru(bpy)_3Cl_2$	470	150 : 1 : 0.002	1.3	0.89	11700	14300	1.16
ZnTPP	530	150 : 1 : 0.005	3	0.83	11000	13400	1.15

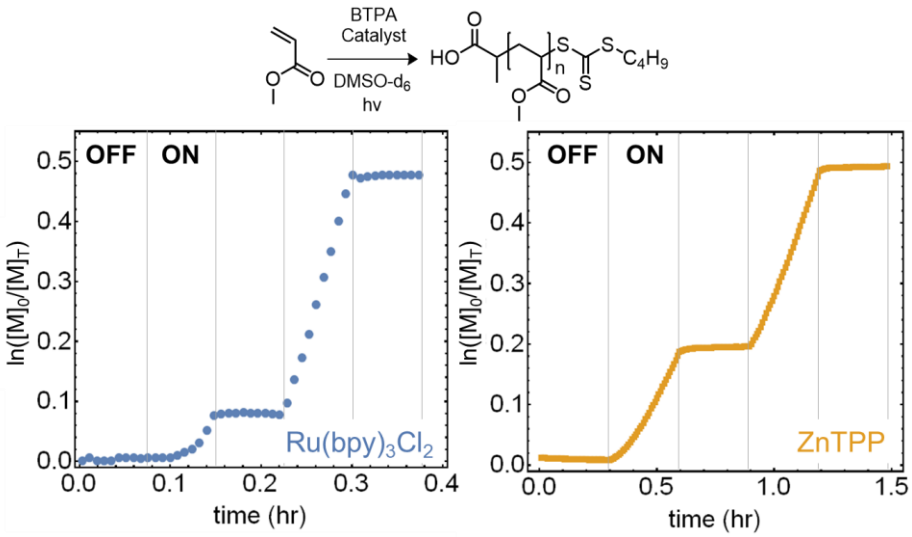

Figure S17: Temporal control cycles for PET-RAFT polymerizations of MA using $Ru(bpy)_3Cl_2$ (left) and ZnTPP (right) under 470 and 530 nm irradiation, respectively. Both polymerizations demonstrate rapid and ideal halting of conversion upon turning off the light.

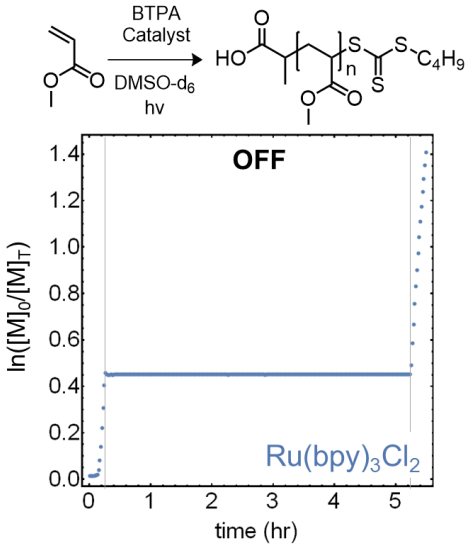

Figure S18: An extended off cycle for the PET-RAFT polymerization of MA using $Ru(bpy)_3Cl_2$ under 470 nm irradiation, clearly demonstrating ideal temporal control over the polymerization. Furthermore, the polymerization could be readily re-started upon further irradiation.

Cu-free ATRP (MMA)

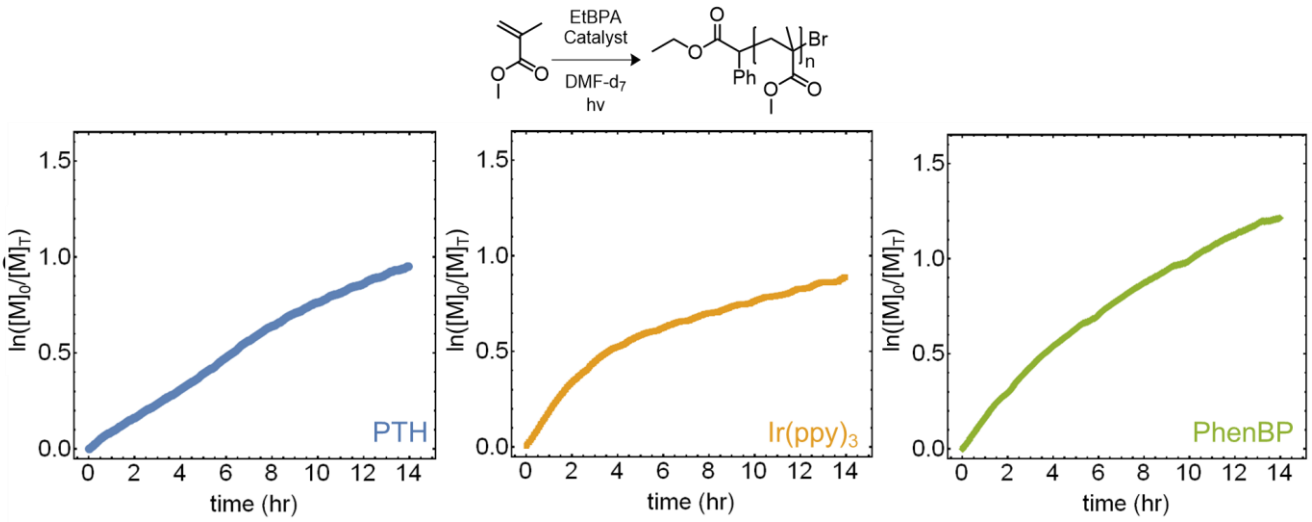

Figure S19: Kinetic traces of Cu-free ATRP of MMA using PTH (left), $Ir(ppy)_3$ (center), and PhenBP under 405, 405, and 470 nm irradiation, respectively.

Table S4: Summary of Cu-free ATRP of MMA and results

catalyst	λ (nm)	[M]:[I]:[catalyst]	time (hr)	conversion	$M_{n,theo}$	$M_{n,exp}$ (SEC)	Đ
PTH	405	150 : 1 : 0.1	14	0.61	9400	11100	1.83
$Ir(ppy)_3$	405	150 : 1 : 0.02	14	0.58	9000	7000	1.77
PhenBP	470	150 : 1 : 0.1	14	0.70	10800	17700	1.55

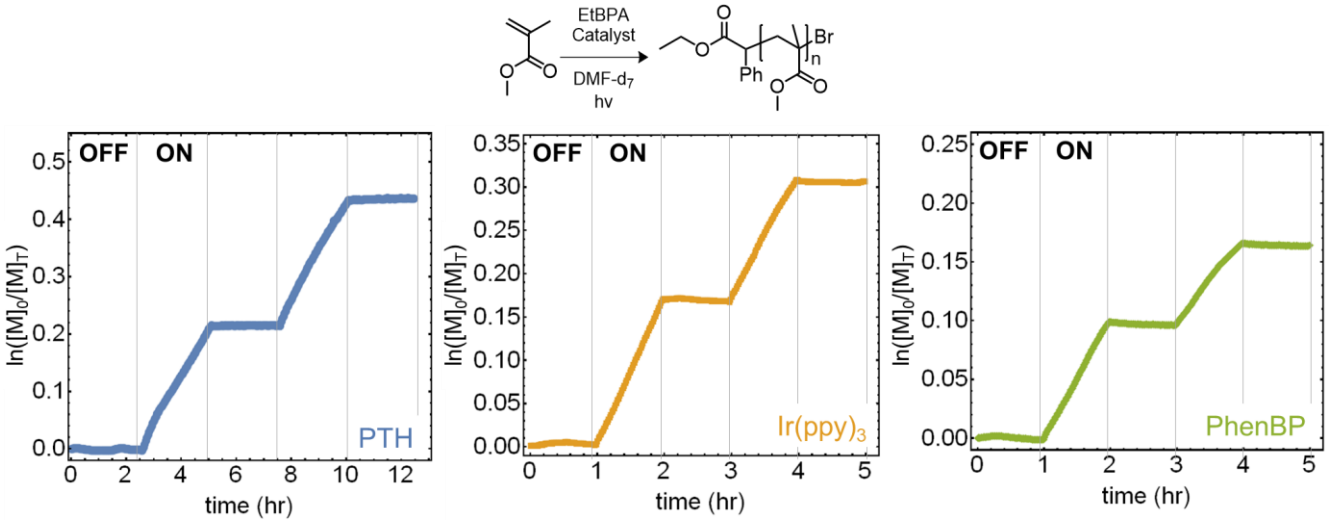

Figure S20: Temporal control cycles of Cu-free ATRP of MMA using PTH (left), $Ir(ppy)_3$ (center), and PhenBP under 405, 405, and 470 nm irradiation, respectively. All three polymerizations demonstrate rapid and ideal halting of conversion upon turning off the light.

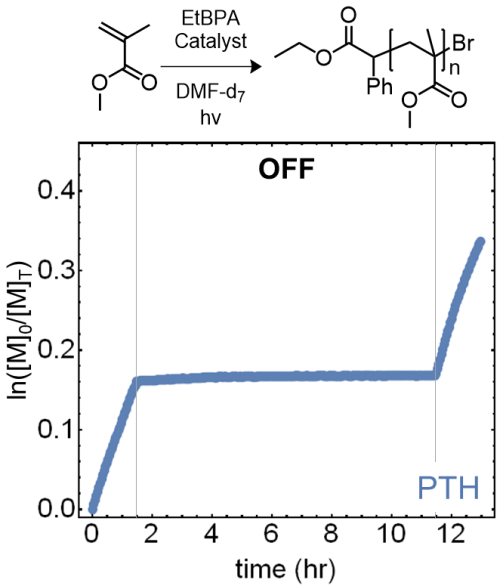

Figure S21: An extended off cycle for the Cu-free ATRP of MMA using PTH under 405 nm irradiation, clearly demonstrating ideal temporal control over the polymerization. Furthermore, the polymerization could be readily re-started upon further irradiation.

Cu-mediated RDRP (MA)

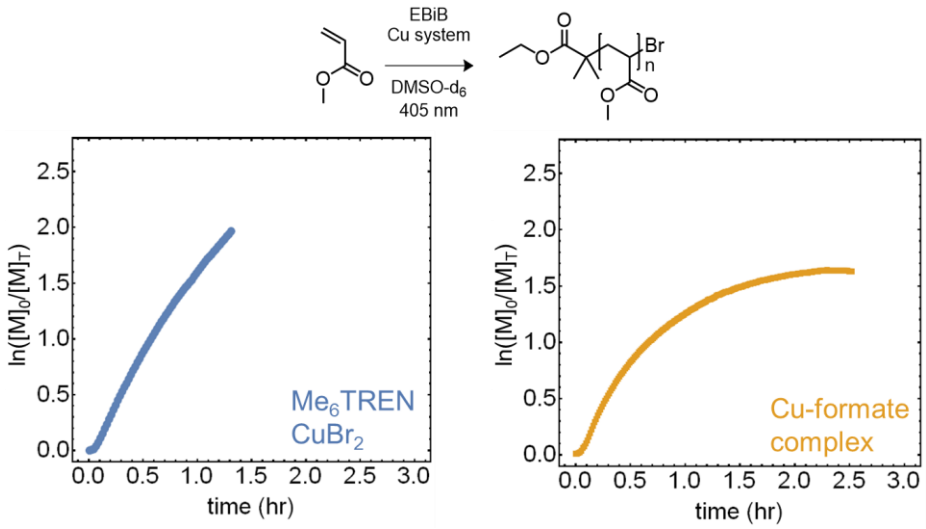

Figure S22: Kinetic traces of the Cu-mediated RDRP of MMA using $CuBr_2$/Me_6TREN (left) and the discrete Cu-formate complex (right) under 405 nm irradiation. Significant termination events can be seen in the case of the complex after ~75% conversion.

Table S5: Summary of Cu-mediated RDRP of MA and results

ligand/catalyst	λ (nm)	[M]:[I]:[$CuBr_2$]:[ligand]	time (hr)	conversion	$M_{n,theo}$	$M_{n,exp}$ (SEC)	Đ
Me_6TREN	405	150 : 1 : 0.02 : 0.12	1.3	0.86	11300	11000	1.09
Cu-formate complex	365	150 : 1 : 0.08 : -----	2.5	0.80	10500	9000	1.15

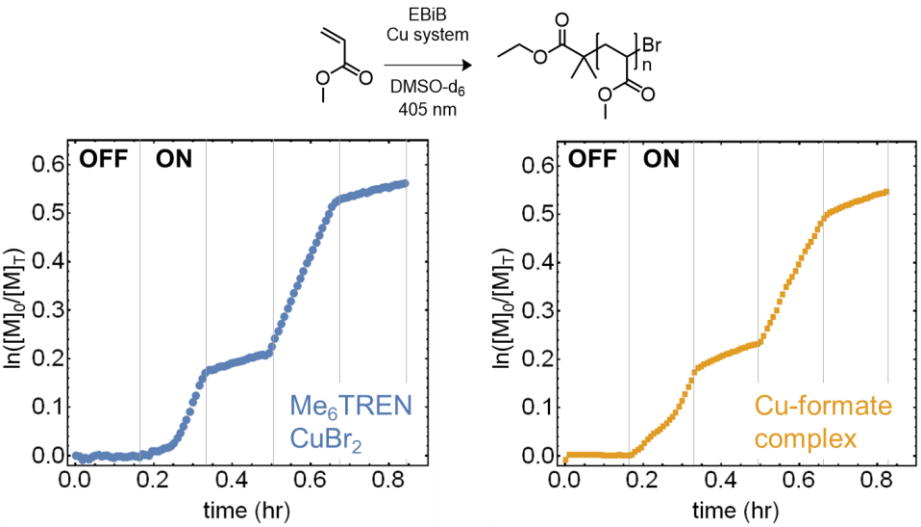

Figure S23: Temporal control cycles for the Cu-mediated RDRP of MMA using $CuBr_2$/Me_6TREN (left) and the discrete Cu-formate complex (right) under 405 nm irradiation. Both Cu-mediated RDRP reactions demonstrate significant and linear growth during off periods after initial irradiation, corresponding to ~10% and ~15% of the on rate, respectively.

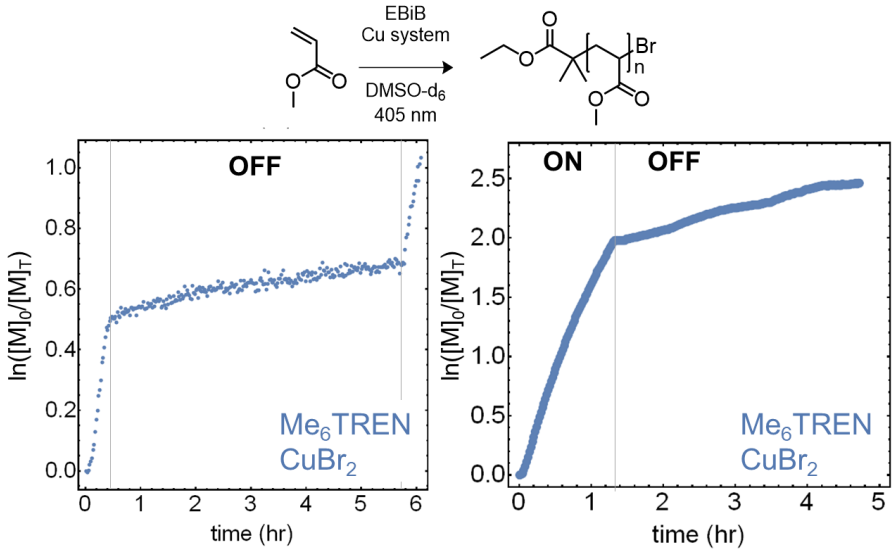

Figure S24: Extended off cycles for the Cu-mediated RDRP of MMA using $CuBr_2$/Me_6TREN under 405 nm irradiation, clearly demonstrating extended linear growth during off periods at intermediate (left) and high (right) conversions. Upon reirradiation, polymerization resumes at a rate comparable to the initial rate (left).

Cu-mediated RDRP (MMA)

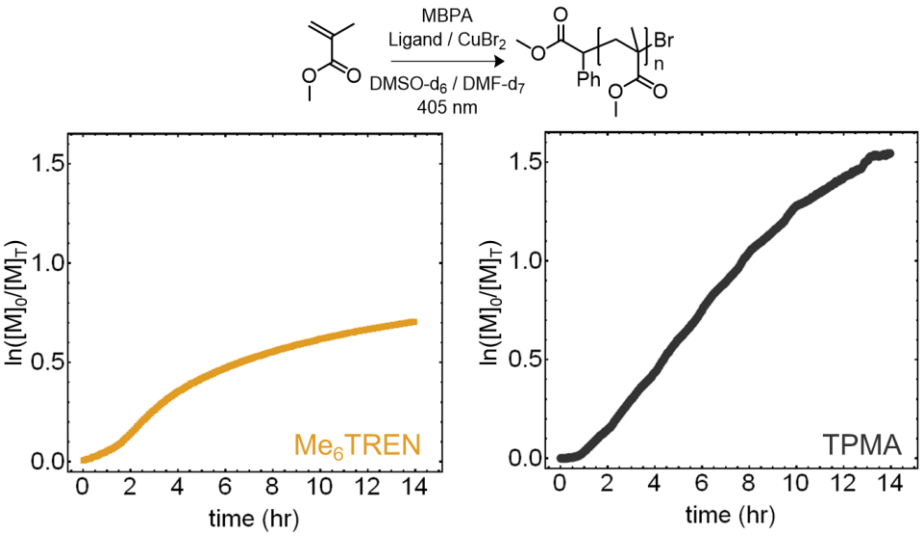

Figure S25: Kinetic traces of the Cu-mediated RDRP of MMA using $CuBr_2$/Me_6TREN (left) in DMF-d_7 and $CuBr_2$/TPMA (right) in DMSO-d_6 under 405 nm irradiation. Both systems demonstrated similar growth at low conversions (below ~35%) making them ideal for comparison in temporal studies.

Table S6: Summary of Cu-mediated RDRP of MMA and results

ligand	λ (nm)	[M]:[I]:[$CuBr_2$]:[ligand]	time (hr)	conversion	$M_{n,theo}$	$M_{n,exp}$ (SEC)	Đ
Me_6TREN	405	150 : 1 : 0.03 : 0.18	14	0.50	7700	5200	1.42
TPMA	405	150 : 1 : 0.03 : 0.18	14	0.79	12100	9400	1.15

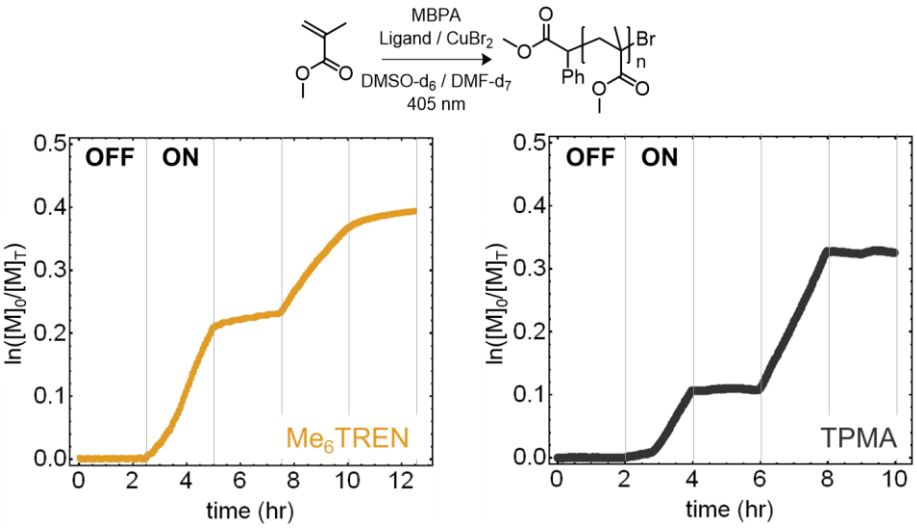

Figure S26: Temporal control of the Cu-mediated RDRP of MMA using $CuBr_2$/Me_6TREN (left) in DMF-d_7 and $CuBr_2$/TPMA (right) in DMSO-d_6 under 405 nm irradiation. Both Cu-mediated RDRP reactions demonstrate growth during off periods after initial irradiation, although in the case of $CuBr_2$/TPMA, this growth only corresponds to ~2% of the on rate.

Cu-mediated RDRP (PEGA)

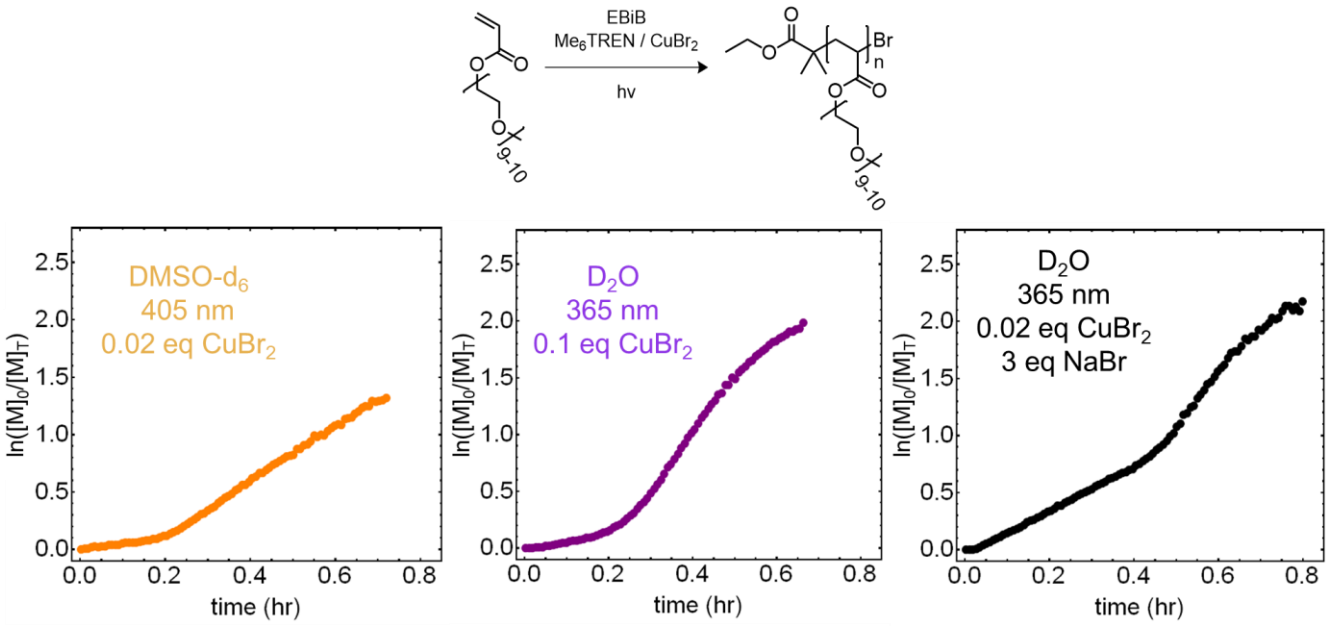

Figure S27: Kinetic traces of the Cu-mediated RDRP of PEGA in DMSO-d_6 and D_2O using $CuBr_2$/Me_6TREN under various conditions.

Table S7: Summary of Cu-mediated RDRP of PEGA and results

solvent	λ (nm)	[M]:[I]:[$CuBr_2$]:[ligand]:[NaBr]	time (hr)	conversion	$M_{n,theo}$	$M_{n,exp}$ (SEC)	Đ
DMSO-d_6	405	150 : 1 : 0.02 : 0.12 : -	0.7	0.73	53000	45500	1.20
D_2O	365	150 : 1 : 0.10 : 0.12 : -	0.7	0.86	62400	48100	1.22
D_2O	365	150 : 1 : 0.02 : 0.12 : 3	0.8	0.89	64600	53200	1.19

References

[1] R. M. Pearson, C. H. Lim, B. G. McCarthy, C. B. Musgrave, G. M. Miyake, *J. Am. Chem. Soc.* **2016**, *138*, 11399–11407.

[2] N. J. Treat, H. Sprafke, J. W. Kramer, P. G. Clark, B. E. Barton, J. Read De Alaniz, B. P. Fors, C. J. Hawker, *J. Am. Chem. Soc.* **2014**, *136*, 16096–16101.

[3] A. Anastasaki, V. Nikolaou, F. Brandford-Adams, G. Nurumbetov, Q. Zhang, G. J. Clarkson, D. J. Fox, P. Wilson, K. Kempe, D. M. Haddleton, *Chem. Commun.* **2015**, *51*, 5626–5629.

[4] N. D. Dolinski, Z. A. Page, F. Eisenreich, J. Niu, S. Hecht, J. Read de Alaniz, C. J. Hawker, *ChemPhotoChem* **2017**, *1*, 125–131.